

Submicrometer Resolution Hard X-Ray Holography with the Asymmetric Bragg Diffraction Microscope

Richard D. Spal

Ceramics Division, National Institute of Standards and Technology, Gaithersburg, Maryland 20899
(Received 17 November 2000)

The asymmetric Bragg diffraction microscope is a novel x-ray microscope which forms a magnified in-line near-field hologram by asymmetric reflection from two crossed flat crystals. In this paper, the optics of the microscope is studied theoretically. The optical transfer function is obtained, and the limiting spatial resolution, rated at 25% modulation transfer, is determined to be $0.30 \mu\text{m}$ at an optimum magnification of $89\times$ with Si crystals, over a wide range of hard x-ray wavelengths. Absorption and phase contrast images can be computed from holograms acquired at several object distances. Application to submicrometer resolution hard x-ray microtomography is envisioned.

DOI: 10.1103/PhysRevLett.86.3044

PACS numbers: 41.50.+h, 07.85.Tt, 42.40.Kw, 61.10.Dp

A quest to achieve $1 \mu\text{m}$ spatial resolution in hard x-ray ($\geq 10 \text{ keV}$) microtomography using synchrotron radiation has spurred the development of detectors optimized for high resolution at the expense of detection efficiency. Currently, a state-of-the-art high resolution detector offers $0.8 \mu\text{m}$ resolution and 3% detection efficiency at 14 keV [1]. Even if a higher resolution detector could be developed, its efficiency might be too low to be generally useful, since low efficiency results in relatively noisy images or long exposures, and the latter may be impractical or produce excessive radiation damage in the object under study, particularly for biological materials.

A promising approach to achieve submicrometer resolution is to magnify the image with an x-ray optic and detect it with a low resolution, high efficiency detector, *thus improving both resolution and efficiency*. The optic must have submicrometer resolution, as well as adequate magnification, efficiency, and image fidelity. Only recently, two hard x-ray optics have demonstrated submicrometer resolution ($0.3 \mu\text{m}$): Fresnel zone plates [2,3] and parabolic compound refractive lenses [4]. However, they have not yet been used in hard x-ray microtomography.

One x-ray optic, the flat asymmetrically cut crystal [5], has been used in hard x-ray microtomography [6–9], but has not demonstrated submicrometer resolution. This optic originated in the field of x-ray diffraction, and its basic imaging properties, e.g., its limiting resolution, have been previously unknown. The purpose of this paper is to theoretically determine its imaging properties, and show they are conducive to performing submicrometer resolution hard x-ray microtomography with synchrotron radiation.

Bragg diffraction from an asymmetrically cut crystal produces one-dimensional magnification. In the simple case of coplanar diffraction [10] shown in Fig. 1, the magnification direction lies in the plane of diffraction [11] and the magnification factor is $\sin(\theta_B + \alpha)/\sin(\theta_B - \alpha)$, where θ_B is the Bragg angle and α is the angle between the Bragg planes and surface. A second diffraction from another crystal with the same magnification factor but

perpendicular plane of diffraction produces uniform two-dimensional magnification.

One-dimensional image magnification was first demonstrated by Kohra [12], who produced radiographic and topographic images at magnifications up to $5.5\times$, using CuK_α radiation (8.0 keV). Compound one-dimensional magnification by double reflection in a grooved crystal was demonstrated by Bonse *et al.* [13], who obtained a resolution of 150 lp/mm (lp stands for line pair and represents a cycle of a spatial frequency) at 10% modulation transfer, using $8.2\times$ (total) magnification and 10.3 keV synchrotron radiation. One-dimensional magnification was applied to computed tomography by Sakamoto *et al.* [6], Bonse *et al.* [7], and Nagata *et al.* [8], using synchrotron radiation.

Two-dimensional image magnification was first demonstrated by Boettinger *et al.* [14], who used two crystals with perpendicular planes of diffraction to produce $25\times$ images with CuK_α radiation. Another setup for two-dimensional magnification using only one crystal (but still two diffractions) was demonstrated by Korytar [15], who produced $6\times$ images with CuK_α radiation. For the latter setup, the problem of finding a pair of surfaces which produce images free of shear distortion was solved analytically by Dobrocka [16].

Using the above two-crystal setup, $79\times$ magnification, and 12.3 keV synchrotron radiation, Kuriyama *et al.* [17] resolved a 420 lp/mm resolution target, implying a resolution of about $1.2 \mu\text{m}$. They also observed Fresnel

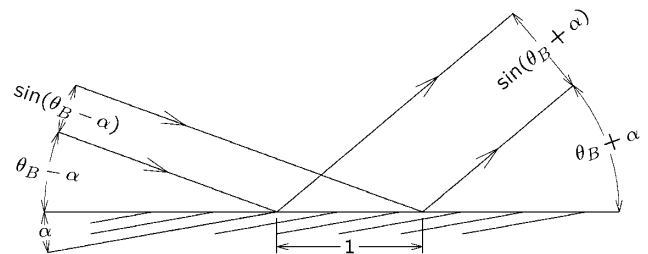


FIG. 1. Asymmetric Bragg diffraction. Slanted lines below crystal's surface represent Bragg planes.

diffraction effects in images, not reported previously, which were studied quantitatively by Spal [18]. Silver [9] performed computed tomography with this instrument using synchrotron radiation.

Only the two-crystal setup with perpendicular planes of diffraction is considered below, and the crystals, subsequently called magnifiers, are assumed to be identical. The incident beam is assumed to be a linearly polarized plane wave of wavelength λ and wave number $k = 2\pi/\lambda$, whose electric field is parallel to the plane of diffraction of the first magnifier. Inelastically scattered and secondary radiation are ignored.

To analyze the microscope, rectangular coordinate systems are established at the object, magnifiers, and detector, as shown in Fig. 2. The positive z axes of these systems follow the incident beam through the microscope, and pass through the centers of the object, magnifier surfaces, and detector. The magnifiers are aligned to pass this beam through the center of their rocking curves. At each magnifier, two coordinate systems are established, denoted by $CS_{\ell h}$ for the ℓ th magnifier, where h is O for the incident beam coordinate system and H for the diffracted beam coordinate system. CS_{1O} and CS_{1H} share the same origin O_1 and y axis, which lie on the magnifier's surface, while CS_{2O} and CS_{2H} share the same origin O_2 and x axis, also on the magnifier's surface. The positive x_{1O} and y_{2O} axes are directed away from the magnifiers. The remaining coordinate systems are indicated by the subscripts o and d , for object and detector. Coordinate systems with parallel z axes (e.g., CS_o and CS_{1O}) also have parallel x and y axes. The y_o axis is assumed to be vertical.

The optical axis is the broken line joining all the origins O_p , and the distance from O_p to O_q measured along the optical axis is denoted Z_{pq} . The magnification factor of the ℓ th magnifier, defined as $|\mathbf{n}_\ell \cdot \hat{\mathbf{z}}_{\ell H} / \mathbf{n}_\ell \cdot \hat{\mathbf{z}}_{\ell O}|$ where \mathbf{n}_ℓ is a vector normal to its surface, is the same for both magnifiers and is denoted m . The vectors $\mathbf{r} = (x, y, z)$ and $\mathbf{s} = (x, y)$ are used to represent arbitrary points and points on the plane $z = 0$, respectively. The vectors $\mathbf{r}' = (x', y', z')$, where $z' = \sqrt{1 - x'^2 - y'^2}$, and $\mathbf{s}' = (x', y')$ are used to represent unit wave vectors and their transverse components, respectively.

It is convenient to decompose the electromagnetic field in each section of the microscope, defined by a segment of the optical axis, into an angular spectrum of plane waves with wave number k . Only paraxial plane waves, i.e., those with $|\mathbf{s}'| \ll 1$, are considered, because others will be strongly attenuated by the magnifiers. Because the elec-

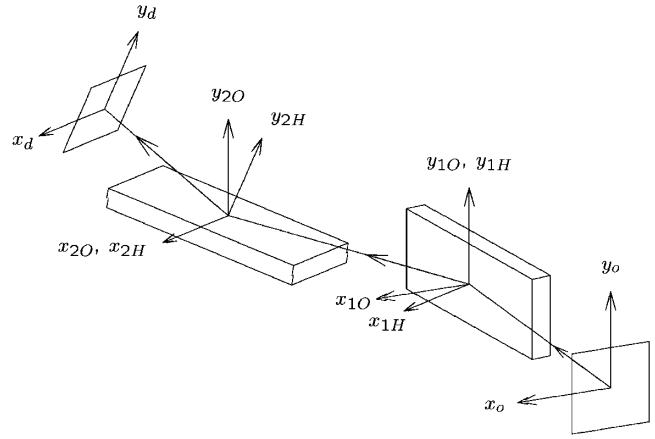


FIG. 2. Microscope, showing magnifiers, object and detector planes, positive x and y axes, and segmented optical axis, with arrows indicating beam direction.

tric field polarization vector of each paraxial wave is very close to $\hat{\mathbf{x}}$, any difference is ignored and the electromagnetic fields are treated as scalar fields. The electric field amplitude $E(\mathbf{r})$ and its angular spectrum $E'(\mathbf{s}')$ are related by $E(\mathbf{r}) = \int d\mathbf{s}' E'(\mathbf{s}') \exp(ik\mathbf{r}' \cdot \mathbf{r})$, where the time dependence of $E(\mathbf{r})$ has been suppressed. $E(\mathbf{r})$ in the section between O_p and O_q , where CS_p and CS_q are parallel, is denoted by $E_p(\mathbf{r}_p)$ when expressed in CS_p coordinates, and by $E_q(\mathbf{r}_q)$ when expressed in CS_q coordinates; e.g., $E_o(\mathbf{r}_o) = E_{1O}(\mathbf{r}_{1O})$ is the electric field amplitude between the object and first magnifier. The angular spectrum of $E_p(\mathbf{r}_p)$ is denoted by $E'_p(\mathbf{s}'_p)$.

The structure of the object determines $E_o(\mathbf{r}_o)$ on the object plane, which in turn determines $E'_o(\mathbf{s}'_o) = \lambda^{-2} \int d\mathbf{s}_o E_o(\mathbf{s}_o, 0) \exp(-ik\mathbf{s}'_o \cdot \mathbf{s}_o)$. Since $\mathbf{r}_o = \mathbf{r}_{1O} + Z_{o1}\hat{\mathbf{z}}_o$, $E'_{1O}(\mathbf{s}'_{1O}) = \exp(ikZ_{o1}z'_o)E'_o(\mathbf{s}'_o)$, where $\mathbf{s}'_{1O} = \mathbf{s}'_o$. The phase factor $\exp(ikZ_{o1}z'_o)$ represents Fresnel diffraction between the object and first magnifier.

At the first magnifier, according to the dynamical theory of x-ray diffraction [19], each component incident wave creates a component diffracted wave, producing $E_{1H}(\mathbf{r}_{1H}) = \int d\mathbf{s}'_{1O} R_1(\mathbf{s}'_{1O}) E'_{1O}(\mathbf{s}'_{1O}) \exp(ik\mathbf{r}'_{1H}(\mathbf{s}'_{1O}) \cdot \mathbf{r}_{1H})$, where $R_1(\mathbf{s}'_{1O})$ is the reflectivity coefficient of the magnifier, $\mathbf{r}'_{1H}(\mathbf{s}'_{1O})$ is implicitly defined by $\mathbf{n}_1 \times (\mathbf{r}'_{1O} + \mathbf{H}/k - \mathbf{r}'_{1H}) = 0$, and \mathbf{H} is the Bragg vector. The corresponding angular spectrum is $E'_{1H}(\mathbf{s}'_{1H}) = J(\mathbf{s}'_{1O}; \mathbf{s}'_{1H}) R_1(\mathbf{s}'_{1O}) E'_{1O}(\mathbf{s}'_{1O})$, where $J(\mathbf{s}'_{1O}; \mathbf{s}'_{1H})$ is the Jacobian of \mathbf{s}'_{1O} with respect to \mathbf{s}'_{1H} .

Assuming, for simplicity of discussion, the magnifier has negligible absorption, which is a good approximation for Si above about 15 keV,

$$R_1(\mathbf{s}'_{1O})/R(0) = \begin{cases} \exp(i \arcsin(2x'_{1O}/\omega_1)) & \text{if } |x'_{1O}| < \omega_1/2 \\ 2ix'_{1O}/\omega_1 - i \operatorname{sgn}(x'_{1O}) \sqrt{(2x'_{1O}/\omega_1)^2 - 1} & \text{otherwise} \end{cases}$$

to first order in \mathbf{s}'_{1O} , where $R(0) = i\sqrt{(\psi_H/\psi_{\bar{H}})/m}$, ψ_H and $\psi_{\bar{H}} = \psi_H^*$ are the Fourier coefficients of the magnifier's dielectric constant at reciprocal lattice vectors \mathbf{H} and $-\mathbf{H}$ respectively, ω_1 is the magnifier's rocking curve width, and

$\text{sgn}(u) = u/|u|$. All component waves are equally attenuated by the factor $m^{-1/2}$ [in $R(0)$] due to magnification. Relative to the central wave ($x'_{10} = 0$), the waves between the rocking curve edges ($|x'_{10}| < \omega_1/2$) are phase shifted monotonically in x'_{10} by up to $\pm\pi/2$ rad but unattenuated. The variable phase shift defocuses the hologram, but because it is nearly linear in x'_{10} for $|x'_{10}| \lesssim \omega_1/4$, low resolution features are simply translated, and only high resolution features are defocused. Relative to the central wave, component waves outside the rocking curve edges are attenuated increasingly with $|x'_{10}|$, asymptotically as $\omega_1/4|x'_{10}|$, and phase shifted by $\text{sgn}(x'_{10})\pi/2$ rad. The increasing attenuation effectively bandlimits the hologram.

As a function of m , the rocking curve width has a maximum value of $\omega_{1\text{max}} = \sqrt{2/(\theta_c \sin 2\theta_B)} |\psi_H| \cos 2\theta_B$ at the optimum magnification factor $m_{\text{opt}} = \sin(2\theta_B)/\sqrt{2}\theta_c$ and optimum glancing angle $\sqrt{2}\theta_c$, where θ_c is the critical angle of total external reflection. These results are derived from a modified two-wave treatment of dynamical diffraction [20–22], which ignores specular reflection but accurately treats the index of refraction correction to Bragg's law. (The standard two-wave treatment fails at grazing incidence, e.g., it incorrectly predicts that $\omega_1 \rightarrow \infty$ as $m \rightarrow \infty$). The modified two-wave treatment is a good approximation at the optimum glancing angle, and has the advantage of yielding simple formulas, but a more rigorous four-wave treatment [23] is available for numerical calculations. The second magnifier has the same m_{opt} , but $\omega_{2\text{max}} = \omega_{1\text{max}}/\cos 2\theta_B$ because the electric field at the second magnifier is polarized perpendicular to the plane of diffraction, rather than parallel to it.

A conservative value for the limiting resolution of the microscope is $\omega_{1\text{max}}/2\lambda$, representing the maximum spatial frequency unattenuated (relative to zero frequency) at the optimum magnification factor m_{opt} . $\omega_{1\text{max}}/2\lambda$ and m_{opt} are nearly independent of wavelength when $\theta_B \lesssim 15^\circ$. At wavelengths below about 1.5 \AA , the limiting resolution is 850 lp/mm ($0.6 \mu\text{m}$) at $m_{\text{opt}} = 89$ for Si (111) reflections, and 1700 lp/mm ($0.3 \mu\text{m}$) at $m_{\text{opt}} = 60$ for Ge (111) reflections. Specified at 25% modulation transfer (i.e., 75% attenuation), the resolutions are twice as good. For (220) reflections at wavelengths below about 1.0 \AA , the resolutions are about 10% worse, and the optimum magnification factors are about 70% greater.

The microscope efficiency, defined as the fraction of the incident beam power reflected by the magnifiers (with no object), is less than 1 due to absorption by the magnifiers, and increases with photon energy, except across an absorption edge. For Si(111) and (220) reflections at the optimum magnification factor, the efficiency is about 50% at 10 keV, and 75% at 15 keV. For Ge (111) and (220) reflections at the optimum magnification factor, the efficiency is about 60% just below the K absorption edge at 11.1 keV, 25% at 18 keV, and 50% at 27 keV.

Combining the above results with analogous ones for the remaining sections of the microscope yields the optical transfer function $\text{OTF}(\mathbf{s}'_o) = \exp(i\Phi(\mathbf{s}'_o)) \times R_1(\mathbf{s}'_{1O})R_2(\mathbf{s}'_{2O})J(\mathbf{s}'_{1O}; \mathbf{s}'_{1H})J(\mathbf{s}'_{2O}; \mathbf{s}'_{2H})$, where $\Phi(\mathbf{s}'_o) = k[Z_{od} - (Z_{o1} + Z_{1d}/m^2)x_o'^2/2 - (Z_{o2} + Z_{2d}/m^2)y_o'^2/2]$ to second order in \mathbf{s}'_o . OTF relates the angular spectra in the object and detector spaces by $E'_d(\mathbf{s}'_d) = \text{OTF}(\mathbf{s}'_o)E'_o(\mathbf{s}'_o)$, and can be used to compute the electric field on the detector plane, given the electric field on the object plane, or vice versa.

The phase factor $\exp(i\Phi)$ in OTF represents Fresnel diffraction. For $m = 1$, Φ reduces to its free space form $kZ_{od}(1 - |\mathbf{s}'_o|^2/2)$. For $m \neq 1$, it is asymmetric with respect to $Z_{o\ell}$ and $Z_{\ell d}$ ($\ell = 1, 2$), and consequently asymmetric with respect to the x and y axes. For $m \gg 1$ and typical $Z_{\ell d}$, horizontal features undergo negligible diffraction after the horizontal magnifier, and vertical features undergo negligible diffraction after the vertical magnifier.

To first order in \mathbf{s}'_o , $\mathbf{s}'_d(\mathbf{s}'_o) = -\mathbf{s}'_o/m$. When $m = 1$, the higher order terms vanish, making $\mathbf{s}'_d(\mathbf{s}'_o)$ strictly linear, which implies the microscope is isoplanatic, i.e., its point spread function is the same over the field of view. When $m \neq 1$, the microscope is nonisoplanatic, because the optical path length between the object plane and detector plane varies over the field of view, making the strength of Fresnel diffraction variable, and hence making the point spread function also variable.

If $E_d(\mathbf{r}_d)$ could be measured on the detector plane, OTF could be used to compute $E_o(\mathbf{r}_o)$ on the object plane, but only the electric field's intensity $I_d(\mathbf{r}_d) = |E_d(\mathbf{r}_d)|^2$ can be measured and not its phase, so half the necessary data is missing. The solution to this phase retrieval problem is to measure $I_d(\mathbf{r}_d)$ at one or more additional values of Z_{o1} to supply the missing data, and solve the nonlinear equations $I_d((\mathbf{s}_d, 0); Z_{o1}^{(\ell)}) = |\int d\mathbf{s}'_d \times \text{OTF}(\mathbf{s}'_o; Z_{o1}^{(\ell)})E'_o(\mathbf{s}'_o) \exp(ik\mathbf{s}'_d \cdot \mathbf{s}_d)|^2$ ($\ell = 1, \dots, N$) for $E'_o(\mathbf{s}'_o)$, where $Z_{o1}^{(\ell)}$ ($\ell = 1, \dots, N$) are the values of Z_{o1} . Absorption and phase contrast images of the object, i.e., $I_o((\mathbf{s}_o, 0))$ and $\arg[E_o((\mathbf{s}_o, 0))]$, may be computed from $E'_o(\mathbf{s}'_o)$. Thus, the microscope can be used for in-line holography with numerical phase retrieval. Hard x-ray in-line holography with numerical phase retrieval was recently used to tomographically reconstruct a phase object [24].

An equivalent in-line holographic imaging problem occurs in electron microscopy, where a series of micrographs with different defocus conditions is used to determine the electron wave function on the object plane by solving corresponding nonlinear equations, given the transfer function [25,26]. For the electron microscope, the transfer function must be experimentally determined. For the x-ray microscope, it can be accurately computed from basic theory because the magnifiers are nearly perfect crystals.

Aberrations due to non-plane-wave illumination must be kept smaller than the limiting resolution in order not to

degrade it. For illumination by a synchrotron radiation source with a crystal monochromator, the aberrations depend on the horizontal and vertical source sizes X_s and Y_s , and the monochromator rocking curve width ω_m . For the purpose of estimating typical aberrations, it is assumed that $X_s = 700 \mu\text{m}$, $Y_s = 40 \mu\text{m}$, the distance from the source to the object Z_{so} is 60 m, the object is close to the first magnifier, $m \gg 1$ (e.g., $m = m_{\text{opt}}$), the magnifiers are just long enough to fully illuminate the detector, and the detector is square with length L_d of 1 cm. The aberration due to the monochromator rocking curve width is roughly $L_d \omega_m / m \sin 2\theta_B$, which is negligible for a monochromator with Si (111) symmetric reflections. The aberration due to the vertical source size is roughly $L_d Y_s / Z_{so} \sin 2\theta_B$, which is also negligible. The aberration due to the horizontal source size is roughly $L_d X_s / Z_{so} \sin 2\theta_B$, which is $0.3 \mu\text{m}$ at $\lambda = 1 \text{ \AA}$ for Si or Ge (111) reflections, and varies nearly as λ^{-1} at shorter wavelengths. This aberration can be reduced by using a slit to effectively decrease X_s , and/or by using (220) reflections instead of (111).

In conclusion, the asymmetric Bragg diffraction microscope can form magnified in-line near-field holograms at submicrometer resolution, with high magnification and high efficiency, over a wide range of hard x-ray wavelengths. Its optical transfer function can be accurately computed from basic theory, because the magnifiers are nearly perfect crystals. As a result, absorption and phase contrast images can be computed from holograms acquired at several object distances. These characteristics make the microscope very promising for performing submicrometer resolution hard x-ray microtomography with synchrotron radiation.

-
- [1] A. Koch, C. Raven, P. Spanne, and A. Snigirev, *J. Opt. Soc. Am. A* **15**, 1940 (1998).
 - [2] B. Lai *et al.*, *Rev. Sci. Instrum.* **66**, 2287 (1995).
 - [3] W. Leitenberger *et al.*, *Opt. Commun.* **180**, 233 (2000).
 - [4] B. Lengeler *et al.*, *Appl. Phys. Lett.* **74**, 3924 (1999).
 - [5] A crystal used in Bragg diffraction is said to be asymmetrically cut when its incident surface is inclined to the Bragg planes, and the diffraction is said to be asymmetric.
 - [6] K. Sakamoto, Y. Suzuki, T. Hirano, and K. Usami, *Jpn. J. Appl. Phys.* **27**, 127 (1988).

- [7] U. Bonse *et al.*, *J. Mater. Sci.* **26**, 4076 (1991).
- [8] Y. Nagata *et al.*, *Res. Nondestruct. Eval.* **4**, 55 (1992).
- [9] M.D. Silver, in *X-Ray Microbeam Technology and Applications*, San Diego, 1995, edited by W. Yun, SPIE Proceedings, Vol. 2516 (SPIE, Bellingham, WA, 1995), pp. 135–147.
- [10] Diffraction is called coplanar when the normal to the incident surface is coplanar with the incident beam wave vector and Bragg vector.
- [11] The plane of diffraction is the plane containing the incident beam wave vector and Bragg vector.
- [12] K. Kohra, in *Proceedings of the Sixth International Conference on X-Ray Optics and Microanalysis*, edited by G. Shinoda, K. Kohra, and T. Ichinokawa (University of Tokyo Press, Tokyo, 1972), pp. 35–45.
- [13] U. Bonse *et al.*, in *X-ray Microscopy III: Proceedings of the Third International Conference, London, 1990*, edited by A. Michette, G. Morrison, and C. Buckley, Springer Series in Optical Sciences Vol. 67 (Springer-Verlag, New York, 1992), pp. 157–176.
- [14] W.J. Boettinger, H.E. Burdette, and M. Kuriyama, *Rev. Sci. Instrum.* **50**, 26 (1979).
- [15] D. Korytar, in *Proceedings of the International Conference on Advanced Methods in X-Ray and Neutron Structure Analysis of Materials, Karlovy Vary, 1987*, edited by J. Hasek (Plenum, New York, 1989), pp. 379–381.
- [16] E. Dobrocka, *J. Appl. Crystallogr.* **24**, 212 (1991).
- [17] M. Kuriyama *et al.*, *J. Res. Natl. Inst. Stand. Technol.* **95**, 559 (1990).
- [18] R.D. Spal, in *National Synchrotron Light Source Annual Report 1991 Volume II*, Brookhaven National Laboratory, edited by S.L. Hulbert and N.M. Lazarz (National Technical Information Service, Springfield, VA, 1991), No. BNL 52317 UC400, p. 275.
- [19] W.H. Zachariasen, *Theory of X-Ray Diffraction in Crystals* (Wiley, New York, 1945).
- [20] F. Rustichelli, *Philos. Mag.* **31**, 1 (1974).
- [21] S. Mazkedian and F. Rustichelli, *Solid State Commun.* **17**, 609 (1975).
- [22] O. Brummer, H.R. Hoche, and J. Nieber, *Phys. Status Solidi A* **37**, 529 (1976).
- [23] S. Kishino and K. Kohra, *Jpn. J. Appl. Phys.* **10**, 551 (1971).
- [24] P. Cloetens *et al.*, *Appl. Phys. Lett.* **75**, 2912 (1999).
- [25] W.O. Saxton, *Computer Techniques for Image Processing in Electron Microscopy* (Academic, New York, 1978).
- [26] M.O. de Beeck, D.V. Dyck, and W. Coene, *Ultramicroscopy* **64**, 167 (1996).